CrossMark

MOLECULAR IMAGING

Applying protein-based amide proton transfer MR imaging to distinguish solitary brain metastases from glioblastoma

Hao Yu[1] · Huiling Lou[2] · Tianyu Zou[1] · Xianlong Wang[1] · Shanshan Jiang[1,4] ·
Zhongqing Huang[3] · Yongxing Du[1] · Chunxiu Jiang[1] · Ling Ma[1] · Jianbin Zhu[1] ·
Wen He[1] · Qihong Rui[1] · Jianyuan Zhou[4] · Zhibo Wen[1]

Abstract

Objectives To determine the utility of amide proton transfer-weighted (APTw) MR imaging in distinguishing solitary brain metastases (SBMs) from glioblastomas (GBMs).

Methods Forty-five patients with SBMs and 43 patients with GBMs underwent conventional and APT-weighted sequences before clinical intervention. The APTw parameters and relative APTw (rAPTw) parameters in the tumour core and the peritumoral brain zone (PBZ) were obtained and compared between SBMs and GBMs. The receiver-operating characteristic (ROC) curve was used to assess the best parameter for distinguishing between the two groups.

Results The $APTw_{max}$, $APTw_{min}$, $APTw_{mean}$, $rAPTw_{max}$, $rAPTw_{min}$ or $rAPTw_{mean}$ values in the tumour core were not significantly different between the SBM and GBM groups ($P = 0.141$, 0.361, 0.221, 0.305, 0.578 and 0.448, respectively).

However, the $APTw_{max}$, $APTw_{min}$, $APTw_{mean}$, $rAPTw_{max}$, $rAPTw_{min}$ or $rAPTw_{mean}$ values in the PBZ were significantly lower in the SBM group than in the GBM group ($P < 0.001$). The $APTw_{min}$ values had the highest area under the ROC curve 0.905 and accuracy 85.2% in discriminating between the two neoplasms.

Conclusion As a noninvasive imaging method, APT-weighted MR imaging can be used to distinguish SBMs from GBMs.

Key Points
• *APTw values in the tumour core were not different between SBMs and GBMs.*
• *APTw values in peritumoral brain zone were lower in SBMs than in GBMs.*
• *The $APTw_{min}$ was the best parameter to distinguish SBMs from GBMs.*

✉ Zhibo Wen
zhibowen@163.com

1 Department of Radiology, Zhujiang Hospital, Southern Medical University, Gongye Road M No.253, Haizhu District, Guangzhou, Guangdong 510282, China

2 Department of Geriatrics, The First People' Hospital of Guangzhou, Guangzhou, Guangdong 510180, China

3 Department of Medical Image Center, Yuebei People's Hospital, Shantou University Medical College, Shantou, Guangdong 515041, China

4 Division of MR Research, Department of Radiology, Johns Hopkins University School of Medicine, 600N. Wolfe Street, Park 336, Baltimore, MD 21287, USA

Abbreviations

GBM	Glioblastoma
SBM	Solitary brain metastases
APT	Amide proton transfer
APTw	APT-weighted
rAPTw	Relative APTw
CEST	Chemical exchange-based saturation transfer
CNAWM	Contralateral normal-appearing white matter
Gd	Gadolinium
H&E	Haematoxylin and eosin
PBZ	Peritumoral brain zone

Introduction

According to the West China Glioma Center (WCGC) and Central Brain tumour Registry of the United States (CBTRUS), metastasis and glioma are the most frequent malignant brain neoplasms, and the incidence rate of both diseases has been increasing in recent decades [1, 2]. The ability to distinguish metastases from glioma is critical because the therapeutic planning and follow-up of these tumours are vastly different [3]. If metastasis is suspected, high-dose Gd should be used to elucidate other metastases in the brain [4], and other parts of the body should be examined. For metastasis therapy, nonsurgical treatment is preferred over conventional surgical resection [5]. However, when glioma is suspected, various advanced MRI techniques are required to detect the true tumour margin, and surgical resection is the first choice [6]. Usually, differentiation between the two neoplasms depends primarily on clinical history, particularly in cases with multiple lesions. However, if the patient's clinical history is uncertain, or the lesion is solitary, the distinction of these neoplasms may be difficult [7]. On conventional MRI, there is substantial overlap between the images of solitary brain metastases (SBMs) and glioblastomas (GBMs), as both manifest similar signal features and contrast enhancement patterns. Previously, investigators worldwide used DWI, PWI, MRS and ASL perfusion imaging to differentiate between these tumours [8–11]. However, the distinction between these two types of tumours still has limited diagnostic specificity.

Amide proton transfer-weighted (APTw) MR imaging was invented by Zhou and van Zijl et al. and is a novel molecular MRI technique based on chemical exchange-based saturation transfer (CEST), which was designed to detect amide protons of endogenous low-concentration mobile proteins and peptides in tissue [12–14]. This technique does not require the use of exogenous contrast agents and is applied to imaging through the exchange between amide protons of mobile proteins and peptides and protons of bulk water. The APTw signals are mainly related to cell density and endogenous mobile proteins and peptides [15–18]. APTw imaging has emerged as a valuable tool for grading brain tumours [18–20] and other cancers that occur in the prostate [21], breast [22, 23] and neck [24, 25]; for distinguishing tumour recurrence from radiation necrosis [26], distinguishing pseudo-progression from true progression in gliomas [27] and differentiating between primary central nervous system lymphomas and glioma [15]; and for characterising cerebral ischaemia [28–30] and Parkinson's disease [31]. However, this technique has not been used to compare SBMs and GBMs. Therefore, the purpose of this study was to evaluate the usefulness of APTw MRI in distinguishing SBMs from GBMs at the molecular level based on their APTw values.

Materials and methods

Study population

The institutional review board of our hospital approved this study, and each patient signed the consent form. From May 2011 to October 2016, 94 patients with SBMs or GBMs were recruited and received conventional and APTw MRI. Data from six patients were excluded because of insufficient image quality due to motion artefacts. Therefore, 88 patients were included in this study. Forty-five patients (33 males, 12 females; age range, 30-74 years; mean age, 56.5 ± 9.2 years) had SBMs confirmed by histopathology ($n = 39$) or clinical diagnosis ($n = 6$). The primary sites of cancers included the lung ($n = 28$), breast ($n = 6$), kidney ($n = 4$), colon ($n = 4$), liver ($n = 2$) and the lymphatic system ($n = 1$), and 43 patients (29 males, 14 females; age range, 18-71 years; mean age, 44.8 ± 13.8 years) had GBMs confirmed by histopathology.

MR imaging

All patients underwent a conventional brain MRI sequence and two-dimensional (2D) APTw sequence on a 3.0-T MRI scanner (Achieva 3.0 T; Philips Medical Systems, Best, The Netherlands) before clinical intervention. A body coil was used for radiofrequency (RF) transmission, and a 16-channel head coil was used for signal reception. Conventional MRI sequences included T_1-weighted [repetition time (ms)/echo time (ms), 400/20], T_2-weighted [repetition time (ms)/echo time (ms), 2800/105] and fluid-attenuated inversion recovery [FLAIR, repetition time (ms)/echo time (ms)/inversion recovery time (ms) 8000/204/2200]. Then, a contrast agent (Gd-DTPA; 0.2 ml/kg body weight; Magnevist; Bayer Schering, Guangzhou, China) was injected through the median cubital vein, and gadolinium-enhanced T_1-weighted images were acquired. Other imaging parameters were as follows: field of view, 240×240 mm^2; slice thickness, 5 mm; gap, 2 mm; matrix, 512×512.

The 2D fat-suppressed, fast spin-echo APTw pulse sequence was performed at one T_2-weighted image slice showing the maximum area of the tumour before the Gd-T_1-weighted image. For saturation, a pulse-train radiofrequency saturation (duration time $= 800$ ms; inter-pulse delay $= 10$ ms; power level $= 2 \mu$T) was used. APTw imaging was performed with a multi-offset (offsets $= 0, \pm 0.25, \pm 0.5, \pm 0.75, \pm 1, \pm 1.5, \pm 2, \pm 2.5, \pm 3, \pm 3.25, \pm 3.5, \pm 3.75, \pm 4, \pm 4.5, \pm 5$ and ± 6 ppm) multi-acquisition protocol. The protocol was repeated eight times at an offset of ± 3.5 ppm to increase the signal-to-noise ratio of the APTw images. In addition, an image that did not exert a saturated pulse was acquired for the signal normalisation, and an image that exerted a saturated pulse at the offset of 15.6 ppm was acquired to calculate the conventional MTR

value. The detailed imaging parameters were as follows: sensitivity-encoding factor = 2, repetition time (s), 3; echo time (ms), 11; field of view, 240×240 mm^2; section thickness, 6 mm; matrix, 128×128; voxel size, $1.65 \times 3.15 \times 6.00$ mm^3. The total acquisition time was 192 s.

Image analysis

The APTw raw data were analysed using interactive data language written in the programme (IDL; Research Systems, Inc., Boulder, CO, USA). First, the normalised saturated signal intensity curve (S_{sat}/S_0, where S_{sat} and S_0 were the signal intensities obtained with and without selective saturation, respectively) as a function of saturation frequency offset, usually called the Z-spectrum, was calculated. The B_0 field inhomogeneity effect was corrected, as described previously [18]. To reduce the contributions from conventional magnetisation transfer contrast and direct saturation of bulk water, a B_0-corrected Z-spectrum was used to analyse the magnetisation transfer ratio asymmetry (MTR_{asym}) as follows: $MTR_{asym} = S_{sat}(\text{-offset})/S_0 - S_{sat}(\text{+offset})/S_0$. The APTw signal was calculated as MTR_{asym} (3.5 ppm).

Images analysis was performed by two experienced neuroradiologists (L.W. and S.J., who have 11 and 10 years of experience in neuroradiology, respectively). The tumour enhancement type and oedema index (EI) were recorded. Five regions of interest (ROIs) were distributed within the Gd-enhancing tumour area, as well as within the peritumoral brain zone (PBZ; peritumoral T_2w hyperintense area, 0.5-2.5 cm from the enhancing tumour area to avoid partial volume contamination) (Fig. 1), based on the Gd-T_1WI and T_2WI co-registered with the APTw image [32]. Large cystic cavities and haemorrhagic components were always excluded. The size of each ROI was 15 pixels. In addition, the contralateral

normal-appearing white matter (CNAWM) was analysed (Fig. 1). For each patient, the APTw values for all ROIs were recorded. Then, the maximum APTw value ($APTw_{max}$), minimum APTw value ($APTw_{min}$) and mean APTw value ($APTw_{mean}$) were determined. To reduce the effect of patient age [33] and other potential experimental errors [34], we also recorded the relative APTw ($rAPTw = APTw - APTw_{CNAWM}$): $rAPTw_{max}$, $rAPTw_{min}$ and $rAPTw_{mean}$.

Pathological data acquisition

The pathologic images were analysed with image analysis software (Image-Pro Plus, version 6.0, Media Cybernetics, Silver Spring, MD, USA). One neuropathologist, blinded to the MRI features, reviewed the haematoxylin and eosin (H&E)-stained biopsy samples from the tumour core and the PBZ of 39 patients with SBM and 43 patients with GBM. The pathological type and tumour grade were recorded according to 2007 WHO classification of tumours of the CNS. The presence of infiltrating cells in the PBZ was also estimated.

Statistical analysis

Statistical analysis performed was statistical analysis software packages (SPSS19.0 and MedCalc v13.1.2.0). The patient's gender was compared between SBMs and GBMs using the chi-square test. Comparison among $APTw_{mean}$ values for the tumour core, PBZ and CNAWM was performed using a one-way analysis of variance (ANOVA) test, followed by multiple comparisons using the Tukey test, to analyse the statistical significance of differences. Comparison between patient's age, $APTw_{CNAWM}$, $APTw_{max}$, $APTw_{min}$, $APTw_{mean}$, $rAPTw_{max}$, $rAPTw_{min}$ or $rAPTw_{mean}$ values for SBMs and GBMs was performed using an independent-samples t-test.
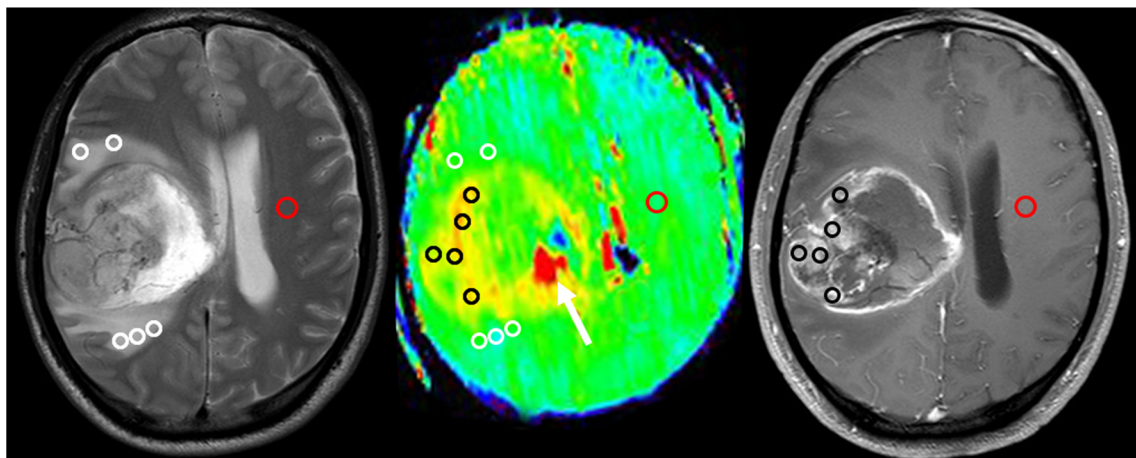

Fig. 1 Example of the placement of ROIs. Five ROIs were placed in the Gd-enhancing tumour part (*black circle*), five ROIs were placed in the peritumoral T_2 hyper-intensity area (*white circle*), and one ROI was placed in the contralateral normal-appearing white matter (*red circle*) based on the co-registered traditional images. The necrosis-related image artefact (*white arrow*) can also be seen

Receiver-operating characteristic (ROC) curves were generated for each parameter to assess the areas under the curves (AUCs) and to determine optimal cut-off values according to Youden's index for the discrimination of SBMs and GBMs. $P < 0.05$ was considered a statistically significant difference for all tests.

Results

There was no gender difference between the SBM and GBM groups ($P = 0.545$). The patient age was higher in the SBM group than in the GBM patients ($P < 0.001$).

Pathological data

In biopsy samples from the PBZ, the tumour cells were present in 29/43 samples; by contrast, 7/39 samples were present in the SBM group.

Comparison of conventional and APTw image features

Forty-five cases of SBMs (45 lesions) were located in the cerebral parenchyma ($n = 36$) and in the cerebellar hemisphere ($n = 9$). Eight cases showed mild oedema, 26 cases showed moderate oedema, and 11 cases showed severe oedema. On the Gd-T_1WI, tumours showed ring-like ($n = 13$), nodular ($n = 22$) or patchy ($n = 10$) enhancement. The tumour cores showed hyperintensities (relative to the CNAWM) on the APTw images, and the hyperintense areas on APTw images were approximately equal to the lesions shown on the Gd-T_1WI. For the 43 cases of GBMs (43 lesions), the lesions were located in the cerebral parenchyma ($n = 35$), brainstem ($n = 2$) and cerebellar hemisphere ($n = 6$). Seven cases showed mild oedema, 30 cases showed moderate oedema, and 6 cases showed severe oedema. In the Gd-T_1WI, the tumours showed ring-like ($n = 24$), nodular ($n = 11$) or patchy ($n = 8$) enhancement. Compared with the CNAWM, the lesions identified by the APTw image were larger than those identified by the Gd-T_1WI. Figure 2 shows an SBM patient, and Fig. 3 shows a GBM patient.

Quantitative APTw image analysis

The APTw value in the CNAWM was significantly lower in SBMs than in GBMs ($0.49\% \pm 0.18\%$ vs. $0.54\% \pm 0.14\%$, $P = 0.046$). The APTw value in the tumour core of SBMs and GBMs was significantly higher than in the CNAWM ($2.76\% \pm 0.71\%$ vs. $0.49\% \pm 0.18\%$, P < 0.001 and $2.94\% \pm 0.67\%$ vs. $0.54\% \pm 0.14\%$, $P < 0.001$). The APTw$_{mean}$ in the PBZ of SBMs and GBMs was significantly higher than in the CNAWM ($1.23\% \pm 0.23\%$ vs. $0.49\% \pm 0.18\%$, $P < 0.001$ and $1.71\% \pm 0.34\%$ vs. $0.54\% \pm 0.14\%$, $P < 0.001$). The

APTw$_{max}$, APTw$_{min}$, APTw$_{mean}$, rAPTw$_{max}$, rAPTw$_{min}$ or rAPTw$_{mean}$ in the tumour core showed significant differences between SBMs and GBMs ($P > 0.05$). By contrast, all parameters in the PBZ were lower in the SBMs than in the GBMs ($P < 0.001$) (Table 1 and Fig. 4).

ROC analyses of the APTw parameter values in the PBZ are summarised in Table 2. The APTw$_{min}$ had the highest AUC of 0.905. When the APTw$_{min}$ of the PBZ was less than 1.21%, the lesion was diagnosed as an SBM. The sensitivity was 84.4%, the specificity was 86.1%, and the accuracy was 85.2% (Table 2).

Discussion

In this study, the gender distribution of patients with SBMs was not significantly different from that of patients with GBMs, although these two tumour types have been shown to be more common in males. Tan et al. [35] found that there was no age difference between the SBM group and high-grade glioma group, but our result shows the SBM patients were significantly older than the GBM patients. As in a previous study [33, 34], the white matter volume was observed to decline after 50 years of age because of demyelination, and the APTw effect due to the myelin basic protein shifted from the oligodendroglia cytoplasm to the myelin sheath. Therefore, we speculated that this was the reason that the APTw parameter value of the CNAWM was lower in the SBM group.

Whether the tumour core can be reliably discriminated between SBMs and GBMs with conventional MRI, even with several advanced MRI techniques such as DWI, PWI, MRS, DTI and ASL, is still controversial [3, 8, 11, 35–37]. Previous studies have shown that APTw MRI can identify the tumour core mainly related to the mobile amide proton content and cell density, which was not relevant to Gd enhancement [16, 18]. This finding is particularly important in the context of the glioma grade, because 10% of patients with glioblastoma may demonstrate non-enhancement on Gd-T_1WI [15], which may miss the central nervous system damage and nephrogenic systemic fibrosis caused by Gd deposition during re-examination [38, 39]. Here we use APTw imaging to distinguish between SBMs and GBMs. Compared with the CNAWM, both SBMs and GBMs exhibited tumour core hyperintensity on APTw images. Quantitative APTw$_{min}$, APTw$_{max}$, APTw$_{mean}$, rAPTw$_{min}$, rAPTw$_{max}$ or rAPTw$_{mean}$ values of the tumour core were not significantly different ($P > 0.05$). It is well known that as malignant tumours SBMs and GBMs exhibit rapid cell proliferation in the tumour core [35] and that the cell density and mobile proteins and peptides are higher than those of the CNAWM. However, the difference in proton content between SBMs and GBMs is expected to be negligible. An investigation of the tumour
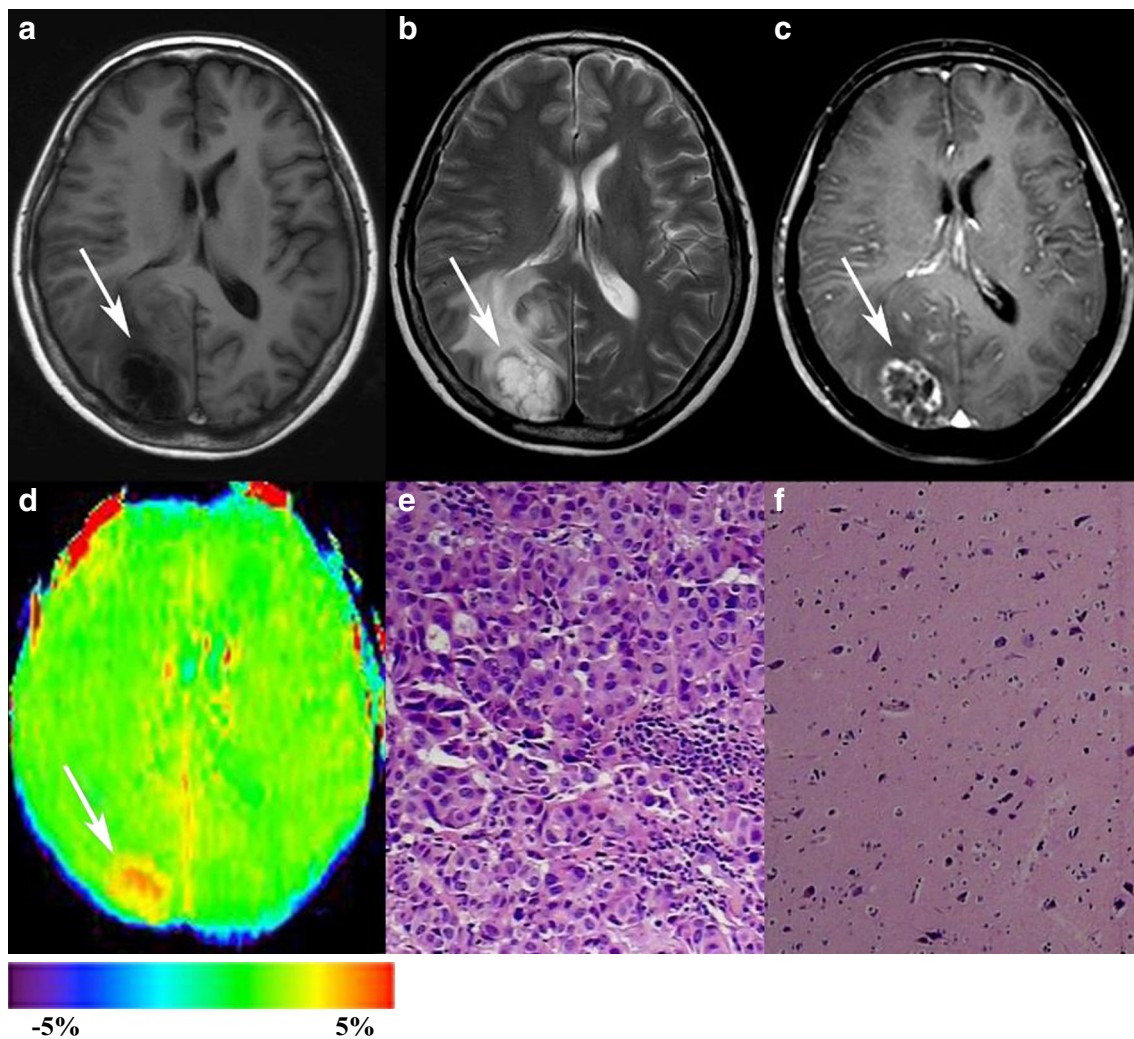
Fig. 2 Results for a 54-year-old female with solitary brain metastasis (*white arrows*). The primary tumour was lung adenocarcinoma. **A**-**C** The tumour was located in the right parietal-occipital lobe with moderate peritumoral oedema. It appears hypointense on T_1WI, hyperintense on T_2WI and ring-like contrast enhanced on Gd-T_1WI. **D** An APTw image shows a relatively homogeneous hyperintense mass (tumour core, APT_{Wmax} =3.55%, APT_{Wmin} =2.87%, APT_{Wmean} =3.34%; peritumoral oedema, APT_{Wmax} =1.72%, APT_{Wmin} =1.57%, APT_{Wmean} =1.63%; APT_{WCNAWM} = 0.74%). **E** H&E-stained sections (×200) of the tumour core show many dense, aggregated cells with atypical nuclei arranged in glandular, nest and cord patterns. **F** H&E-stained sections (×100) of the peritumoral oedema show the degeneration of nerve cells and the proliferation of glial cells, but no tumour cells are found

core using APTw MRI cannot provide useful information to distinguishing SBMs from GBMs.

The peritumoral brain zone (PBZ) is defined radiologically as the non-enhancing brain area of several centimetres in width surrounding the tumour in Gd-T_1WI. Usually, this area shows hyper-intensity on T_2WI and FLAIR images because of vasogenic oedema [40]; as the blood-brain barrier breaks down, capillary permeability increases, a pressure gradient from the vasculature to the extracellular environment is formed, and many intravascular proteins penetrate into the extra-cellular space [41]. In this study, the APTw value in the PBZ of SBMs and GBMs was significantly higher than in the CNAWM ($P < 0.001$). It is interesting to note that the values of $APTw_{min}$, $APTw_{max}$, $APTw_{mean}$, $rAPTw_{min}$,

$rAPTw_{max}$ or $rAPTw_{mean}$ in the SBM group were significantly lower than in the GBM group ($P < 0.001$). In metastasis brain tumours, PBZ T_2 hyperintensity mainly reflects vasogenic oedema [7, 35]. In the GBMs, it is hypothesised that specific cells and inflammatory cells infiltrate into the PBZ [40, 42–44] and that the PBZ T_2 hyperintensity reflects more than vasogenic oedema. Technically, the APTw effect is due to the shift of the amide proton from mobile proteins and peptides to the water proton [12]. In the PBZ of GBMs, other than intravascular proteins, because of the infiltration of tumour cells and inflammatory cells, the tumour-related molecules and inflammatory mediators are also retained in the extra-cellular space of the PBZ [41, 45], and the mobile protein and peptide content may be higher than in SBMs. The pathological
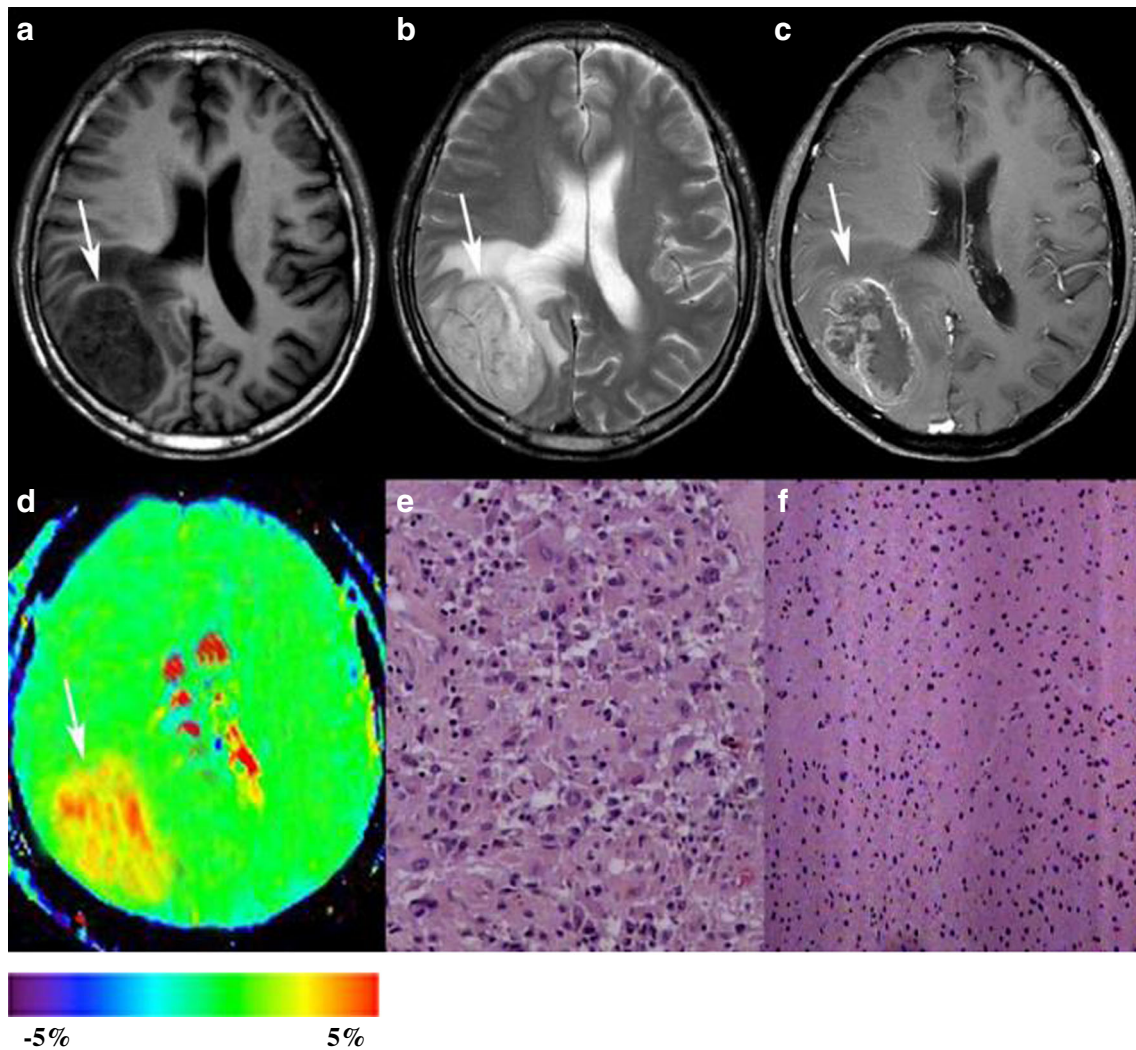
Fig. 3 Results for a 67-year-old male with glioblastoma. **A-C** The tumour is located in the right occipital lobe with mild peritumoral oedema. The tumour appears hypointense on the T_1WI, hyperintense on the T_2WI and ring-like contrast enhanced on the Gd-T_1WI. **D** An APT_W image shows a heterogeneously hyperintense mass (tumour core: APT_{Wmax} =3.87%, APT_{Wmin} =2.96%, APT_{Wmean} =3.61%; peritumoral oedema: APT_{Wmax} =2.09%, APT_{Wmin} =1.63%, APT_{Wmean} =1.89%; APT_{WCNAWM} =0.57%). **E** H&E-stained sections (×200) of the tumour core show many multinucleated atypical tumour cells with relatively abundant cytoplasm. **F** H&E-stained sections (×100) of the peritumoral oedema show proliferating glial cells and a number of cells with atypical nuclei

Table 1 APT_W parameter values of the tumour core and peritumoral brain zone

Parameter	Tumour core		P	Peritumoral brain zone		P
	SBM	GBM		SBM	GBM	
$APTw_{max}$	2.98% ± 0.74%	3.22% ± 0.75%	0.141	1.56% ± 0.22%	1.98% ± 0.31%	<0.001
$APTw_{min}$	2.53% ± 0.70%	2.66% ± 0.63%	0.361	0.98% ± 0.25%	1.48% ± 0.34%	<0.001
APT_{Wmean}	2.76% ± 0.71%	2.94% ± 0.67%	0.221	1.23% ± 0.23%	1.71% ± 0.34%	<0.001
$rAPTw_{max}$	2.51% ± 0.79%	2.67% ± 0.73%	0.305	1.09% ± 0.22%	1.43% ± 0.31%	<0.001
$rAPTw_{min}$	2.03% ± 0.71%	2.10% ± 0.58%	0.578	0.51% ± 0.29%	0.95% ± 0.30%	<0.001
$rAPTw_{mean}$	2.28% ± 0.76%	2.40% ± 0.65%	0.448	0.76% ± 0.27%	1.17% ± 0.32%	<0.001

(r)$APTW_{max}$, (relative) amide proton transfer-weighted max; (r)$APTW_{min}$, (relative) amide proton transfer-weighted min; (r)$APTW_{mean}$, (relative) amide proton transfer-weighted mean; SBM, solitary brain metastasis; GBM, glioblastoma

Fig. 4 Comparisons of the amide proton transfer-weighted (APTw) parameter (APTwmax, APTwmean, APTwmin, rAPTwmax, rAPTwmean, rAPTwmin) values measured in the peritumoral oedema for GBMs and SBMs; APTw values in the SBM group are significantly lower than those in the GBM group ($P < 0.001$)
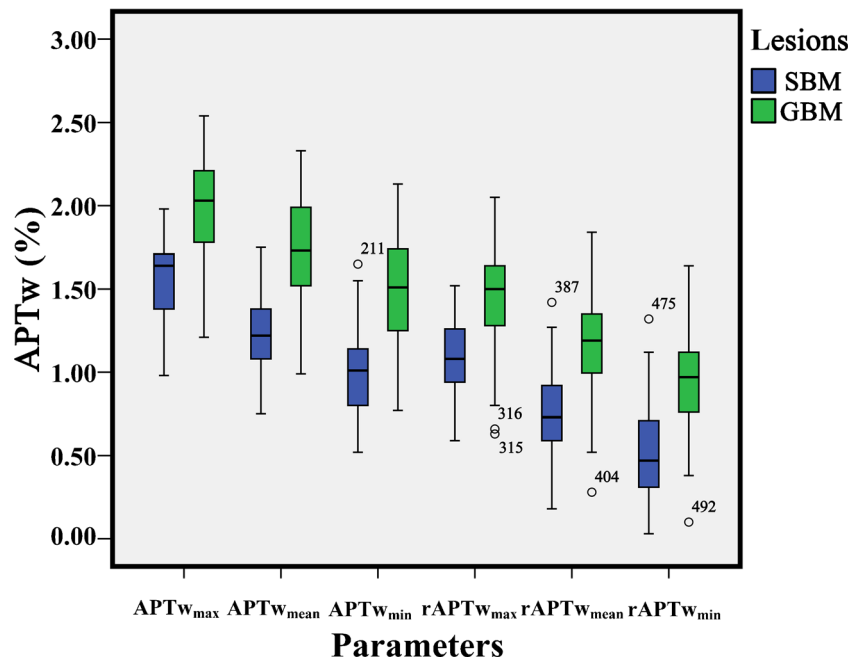
examination of PBZ supports this hypothesis. Notably, the APTw value in the PBZ of SBMs was significantly higher than in the CNAWM. We speculate that, as the intravascular proteins penetrate into the extra-cellular space of the PBZ, the amide proton content exceeds that in the CNAWM [41].

According to ROC curve analysis, the APTw$_{min}$ had the highest AUC (0.905) and accuracy (85.2%) for distinguishing between SBMs and HGGs. For the 88 participants in this study, the accuracy for differentiating SBMs from GBMs was 51.6% (by Y.D., a junior radiologist with 3 years of experience in brain imaging, blinded to the pathology reports, based on conventional MRI sequences) and 79.5% (according to official radiology reports, performed by senior neuro-radiologists in our department). Compared with conventional MRI, protein-based APT$_W$ imaging can improve the accuracy for discriminating between SBMs and GBMs.

On conventional MRI images, although glioma cells infiltrate into the PBZ, the blood-brain barrier does not break down,

and enhancement is not observed in Gd-T$_1$WI [18]. However, the cell density and mobile proteins and peptides in the PBZ increased; in the PBZ of GBMs, the APTw value was higher closer to the tumour core than the APTw value in the CNAWM; thus, the APTw MRI, which is based on amide protons, may provide new insights into the evaluation of the extent of GBM cell infiltration in the PBZ on a molecular level.

However, this study has several limitations. First, the sample size of the metastasis group mainly involves the metastasis of lung cancer. A larger sample size that includes metastases of more primary cancers is required for more reliable results. Second, the APT-weighted sequence covered only one slice, and the MRI signal changes in other tumour regions could not be evaluated in the present study. Third, in the current study, the voxel size of the APT-weighted sequence was relatively large (due to the small APT effect), which may have led to homogeneous APTw hyperintensities due to the large partial volume effect.

Table 2 ROC analysis results of APTw parameter values in the peritumoral oedema

Parameter	AUC	95% CI	P-value	Cut-off	Sensitivity	Specificity	Accuracy
APT$_{Wmax}$	0.856	0.764-0.921	$P < 0.001$	1.85%	93.3%	69.8%	79.5%
APT$_{Wmin}$	0.905	0.824-0.957	$P < 0.001$	1.21%	84.4%	86.1%	85.2%
APT$_{Wmean}$	0.868	0.779-0.931	$P < 0.001$	1.46%	86.7%	81.4%	81.8%
rAPT$_{Wmax}$	0.829	0.734-0.901	$P < 0.001$	1.27%	80.0%	76.7%	76.1%
rAPT$_{Wmin}$	0.864	0.774-0.927	$P < 0.001$	0.71%	77.8%	85.5%	79.5%
rAPT$_{Wmean}$	0.841	0.748-0.911	$P < 0.001$	1.09%	82.2%	74.4%	77..3%

(r)APTW$_{max}$, (relative)amide proton transfer-weighted max; (r)APTW$_{min}$, (relative)amide proton transfer-weighted min; (r)APTW$_{mean}$, (relative)amide proton transfer-weighted mean

In conclusion, APT-weighted MRI can differentiate between solitary brain metastases and glioblastoma, which indicates that comparisons in APTw parameters in the peritumoral oedema may be useful for differentiating between SBMs and GBMs. The APTw$_{min}$ has the highest sensitivity, specificity and accuracy. As a safe and completely non-invasive imaging technique, APT-weighted MRI could be a supplement to improve the preoperative diagnosis of SBMs and GBMs in the clinic.

Compliance with ethical standards

Guarantor The scientific guarantor of this publication is Zhibo Wen, MD.

Conflict of interest The authors of this manuscript declare no relationships with any companies, whose products or services may be related to the subject matter of the article.

Statistics and biometry No complex statistical methods were necessary for this article.

Informed consent Written informed consent was obtained from all subjects (patients) in this study.

Ethical approval Institutional Review Board approval was obtained.

Methodology
• retrospective
• diagnostic or prognostic study
• performed at one institution

References

1. Wang X, Chen JX, Zhou Q et al (2016) Statistical report of central nervous system tumors histologically diagnosed in the Sichuan Province of China from 2008 to 2013: a West China Glioma Center Report. Ann Surg Oncol. doi:10.1245/s10434-016-5410-1

2. Ostrom QT, Gittleman H, Fulop J et al (2015) CBTRUS statistical report: primary brain and central nervous system tumors diagnosed in the United States in 2008-2012. Neuro-Oncology 17:v1–iv62

3. Blanchet L, Krooshof PW, Postma GJ et al (2011) Discrimination between metastasis and glioblastoma multiforme based on morphometric analysis of MR images. AJNR Am J Neuroradiol 32:67–73

4. Yuh WT, Engelken JD, Muhonen MG, Mayr NA, Fisher DJ, Ehrhardt JC (1992) Experience with high-dose gadolinium MR imaging in the evaluation of brain metastases. AJNR Am J Neuroradiol 13:335–345

5. Owonikoko TK, Arbiser J, Zelnak A et al (2014) Current approaches to the treatment of metastatic brain tumours. Nat Rev Clin Oncol 11:203–222

6. Wen PY, Kesari S (2008) Malignant gliomas in adults. N Engl J Med 359:492–507

7. Lee EJ, Ahn KJ, Lee EK, Lee YS, Kim DB (2013) Potential role of advanced MRI techniques for the peritumoural region in differentiating glioblastoma multiforme and solitary metastatic lesions. Clin Radiol 68:e689–e697

8. Han CK, Huang SM, Guo JF, Zhuang XJ, Han HW (2015) Use of a high b-value for diffusion weighted imaging of peritumoral regions to differentiate high-grade gliomas and solitary metastases. J Magn Reson Imaging 42:80–86

9. Abe T, Mizobuchi Y, Sako W et al (2015) Clinical significance of discrepancy between arterial spin labeling images and contrast-enhanced images in the diagnosis of brain tumors. Magn Reson Med Sci 14:313–319

10. Caivano R, Lotumolo A, Rabasco P et al (2013) 3 Tesla magnetic resonance spectroscopy: cerebral gliomas vs. metastatic brain tumors. Our experience and review of the literature. Int J Neurosci 123:537–543

11. Mouthuy N, Cosnard G, Abarca-Quinones J, Michoux N (2012) Multiparametric magnetic resonance imaging to differentiate high-grade gliomas and brain metastases. J Neuroradiology Journal de neuroradiologie 39:301–307

12. Zhou J, Lal B, Wilson DA, Laterra J, van Zijl PC (2003) Amide proton transfer (APT) contrast for imaging of brain tumors. Magn Reson Med 50:1120–1126

13. Zhou J, Payen JF, Wilson DA, Traystman RJ, van Zijl PC (2003) Using the amide proton signals of intracellular proteins and peptides to detect pH effects in MRI. Nat Med 9:1085–1090

14. van Zijl PCM, Yadav NN (2011) Chemical exchange saturation transfer (CEST): what is in a name and what Isn't? Magn Reson Med 65:927–948

15. Jiang SS, Yu H, Wang XL et al (2016) Molecular MRI differentiation between primary central nervous system lymphomas and high-grade gliomas using endogenous protein-based amide proton transfer MR imaging at 3 Tesla. Eur Radiol 26:64–71

16. Zhou J, Zhu H, Lim M et al (2013) Three-dimensional amide proton transfer MR imaging of gliomas: initial experience and comparison with gadolinium enhancement. J Magn Reson Imaging 38:1119–1128

17. Togao O, Kessinger CW, Huang G et al (2013) Characterization of lung cancer by amide proton transfer (APT) imaging: an in-vivo study in an orthotopic mouse model. Plos One 8:e77019

18. Wen ZB, Hu SG, Huang FH et al (2010) MR imaging of high-grade brain tumors using endogenous protein and peptide-based contrast. Neuroimage 51:616–622

19. Togao O, Hiwatashi A, Yamashita K et al (2016) Grading diffuse gliomas without intense contrast enhancement by amide proton transfer MR imaging: comparisons with diffusion- and perfusion-weighted imaging. Eur Radiol. doi:10.1007/s00330-016-4328-0:1-11

20. Sakata A, Okada T, Yamamoto A et al (2015) Grading glial tumors with amide proton transfer MR imaging: different analytical approaches. J Neuro-Oncol 122:339–348

21. Jia G, Abaza R, Williams JD et al (2011) Amide proton transfer MR imaging of prostate cancer: a preliminary study. J Magn Reson Imaging 33:647–654

22. Klomp DWJ, Dula AN, Arlinghaus LR et al (2013) Amide proton transfer imaging of the human breast at 7T: development and reproducibility. NMR Biomed 26:1271–1277

23. Dula AN, Arlinghaus LR, Dortch RD et al (2013) Amide proton transfer imaging of the breast at 3 T: Establishing reproducibility

and possible feasibility assessing chemotherapy response. Magn Reson Med 70:216–224

24. Wang J, Weygand J, Hwang KP et al (2016) Magnetic resonance imaging of glucose uptake and metabolism in patients with head and neck cancer. Scientific reports 6:30618

25. Yuan J, Chen S, King AD et al (2014) Amide proton transfer-weighted imaging of the head and neck at 3 T: a feasibility study on healthy human subjects and patients with head and neck cancer. NMR Biomed 27:1239–1247

26. Zhou JY, Tryggestad E, Wen ZB et al (2011) Differentiation between glioma and radiation necrosis using molecular magnetic resonance imaging of endogenous proteins and peptides. Nat Med 17:130–U308

27. Ma B, Blakeley JO, Hong X et al (2016) Applying amide proton transfer-weighted MRI to distinguish pseudoprogression from true progression in malignant gliomas. J Magn Reson Imaging 44:456–462

28. Tietze A, Blicher J, Mikkelsen IK et al (2014) Assessment of ischemic penumbra in patients with hyperacute stroke using amide proton transfer (APT) chemical exchange saturation transfer (CEST) MRI. NMR Biomed 27:163–174

29. Tee YK, Harston GWJ, Blockley N et al (2014) Comparing different analysis methods for quantifying the MRI amide proton transfer (APT) effect in hyperacute stroke patients. NMR Biomed 27:1019–1029

30. Zhao XN, Wen ZB, Huang FH et al (2011) Saturation power dependence of amide proton transfer image contrasts in human brain tumors and strokes at 3 T. Magn Reson Med 66:1033–1041

31. Li CM, Peng S, Wang R et al (2014) Chemical exchange saturation transfer MR imaging of Parkinson's disease at 3 Tesla. Eur Radiol 24:2631–2639

32. Zhang Y, Heo HY, Lee DH et al (2016) Selecting the reference image for registration of CEST series. J Magn Reson Imaging 43:756–761

33. Zhang H, Kang H, Zhao X et al (2016) Amide proton transfer (APT) MR imaging and magnetization transfer (MT) MR imaging of pediatric brain development. Eur Radiol 26:3368–3376

34. Allen JS, Bruss J, Brown CK, Damasio H (2005) Normal neuroanatomical variation due to age: the major lobes and a parcellation of the temporal region. Neurobiol Aging 26:1245–1260

35. Tan Y, Wang XC, Zhang H et al (2015) Differentiation of high-grade-astrocytomas from solitary-brain-metastases: comparing diffusion kurtosis imaging and diffusion tensor imaging. Eur J Radiol 84:2618–2624

36. Crisi G, Orsingher L, Filice S (2013) Lipid and macromolecules quantitation in differentiating glioblastoma from solitary metastasis: a short-echo time single-voxel magnetic resonance spectroscopy study at 3 T. J Comput Assist Tomogr 37:265–271

37. Lee EJ, terBrugge K, Mikulis D et al (2011) Diagnostic value of peritumoral minimum apparent diffusion coefficient for differentiation of glioblastoma multiforme from solitary metastatic lesions. AJR Am J Roentgenol 196:71–76

38. Ramalho J, Castillo M, AlObaidy M et al (2015) High signal intensity in globus pallidus and dentate nucleus on unenhanced T1-weighted MR images: evaluation of two linear gadolinium-based contrast agents. Radiology 276:836–844

39. Collidge TA, Thomson PC, Mark PB et al (2007) Gadolinium-enhanced MR imaging and nephrogenic systemic fibrosis: retrospective study of a renal replacement therapy cohort. Radiology 245:168–175

40. Lemee JM, Clavreul A, Aubry M et al (2015) Characterizing the peritumoral brain zone in glioblastoma: a multidisciplinary analysis. J Neuro-Oncol 122:53–61

41. Oh J, Cha S, Aiken AH et al (2005) Quantitative apparent diffusion coefficients and T2 relaxation times in characterizing contrast enhancing brain tumors and regions of peritumoral edema. J Magn Reson Imaging 21:701–708

42. Goplen D, Bougnaud S, Rajcevic U et al (2010) Alpha B-Crystallin is elevated in highly infiltrative apoptosis-resistant glioblastoma cells. Am J Pathol 177:1618–1628

43. Parney IF, Waldron JS, Parsa AT (2009) Flow cytometry and in vitro analysis of human glioma-associated macrophages. Laboratory investigation Journal of neurosurgery 110:572–582

44. Frieboes HB, Zheng X, Sun CH, Tromberg B, Gatenby R, Cristini V (2006) An integrated computational/experimental model of tumor invasion. Cancer Res 66:1597–1604

45. Fazi B, Felsani A, Grassi L et al (2015) The transcriptome and miRNome profiling of glioblastoma tissues and peritumoral regions highlights molecular pathways shared by tumors and surrounding areas and reveals differences between short-term and long-term survivors. Oncotarget 6:22526–22552